applied sciences

MDPI

Review

Wavefront Shaping and Its Application to Enhance Photoacoustic Imaging

Zhipeng Yu, Huanhao Li and Puxiang Lai *

Department of Biomedical Engineering, The Hong Kong Polytechnic University, Hong Kong 999077, China; yu.zh.yu@polyu.edu.hk (Z.Y.); huanhao.li@connect.polyu.hk (H.L.)

* Correspondence: puxiang.lai@polyu.edu.hk; Tel.: +852-3400-8900

Received: 14 October 2017; Accepted: 30 October 2017; Published: 19 December 2017

Abstract: Since its introduction to the field in mid-1990s, photoacoustic imaging has become a fast-developing biomedical imaging modality with many promising potentials. By converting absorbed diffused light energy into not-so-diffused ultrasonic waves, the reconstruction of the ultrasonic waves from the targeted area in photoacoustic imaging leads to a high-contrast sensing of optical absorption with ultrasonic resolution in deep tissue, overcoming the optical diffusion limit from the signal detection perspective. The generation of photoacoustic signals, however, is still throttled by the attenuation of photon flux due to the strong diffusion effect of light in tissue. Recently, optical wavefront shaping has demonstrated that multiply scattered light could be manipulated so as to refocus inside a complex medium, opening up new hope to tackle the fundamental limitation. In this paper, the principle and recent development of photoacoustic imaging and optical wavefront shaping are briefly introduced. Then we describe how photoacoustic signals can be used as a guide star for in-tissue optical focusing, and how such focusing can be exploited for further enhancing photoacoustic imaging in terms of sensitivity and penetration depth. Finally, the existing challenges and further directions towards in vivo applications are discussed.

Keywords: photoacoustic imaging; optical scattering; optical diffusion limit; penetration depth; wavefront shaping; iterative optimization; transmission matrix; Grueneisen effect; noninvasive internal guide star

1. Introduction

High-resolution optical imaging has recently seen more and more biomedical applications, such as optical coherence tomography (OCT) for optometry [1], confocal microscopy for cytobiology research [2], two- or three-photon microscopy for deep tissue imaging [3–8], as well as stimulated emission depletion (STED) microscopy and photo-activated localization microscopy (PALM) for super-resolution imaging of single molecules [9,10]. In almost all of these applications, photons, whether illuminating or excited ones, need to propagate some distance in tissue. Therefore, the capability of focusing light plays an essential role, largely determining the sensitivity and spatial resolution of these techniques. It would be ideal if human tissues were as transparent as those of a jelly fish or X-ray fish. However, due to the inhomogeneities of the refractive index among different cells and organelles in tissue [11], photons are multiply scattered along their respective optical paths. As a result, an incident optical beam spreads out and becomes diffusive very quickly as it travels deep into tissue (typically ~1 mm beneath human skin for visible and near-infrared light). Beyond this so-called optical diffusion limit, optical focus can hardly be formed by using lenses or objects; instead, if the coherence length of light is sufficiently long, optical speckle patterns are developed within or behind a thick biological tissue sample. Moreover, because of the strong scattering, the in situ optical fluence also decays rapidly. These two folds pose a fundamental limitation to the aforementioned high-resolution techniques to be viable only within superficial depths (e.g., less than 100–200 micrometers).

Recently, photoacoustic (PA) imaging has been introduced to tackle the diffusion-induced resolution barrier in deep tissue [11–15]. This technique is based on the so-called PA effect [16–18], which mainly consists of four steps: first, tissue molecules in the region of interest (ROI) within the sample absorb pulsed light (no matter if it is in ballistic or diffusive form); the absorbed optical energy is converted to heat, causing local the temperature to increases; ultrasonic waves are generated due to thermal expansion; finally, these ultrasonic waves (typically around the order of MHz if the exiting light pulse width is several nanoseconds) can be detected by one or a series of ultrasound transducers mounted outside the sample. Since ultrasonic waves are scattered almost 1000 times less than light is in tissue (unless otherwise mentioned, we always mean soft tissue in the context), they can be used to reconstruct an image of the absorbing ROI with an acoustic resolution [19–27]. As the generation of such PA signals does not distinguish ballistic or diffusive exciting light formations, it allows for a penetration depth far exceeding the optical diffusion limit. On the other hand, if only shallow tissue depths (e.g., within one transport mean free path) are sought, where ballistic or quasi-ballistic photons dominate, the optical spot size can be much smaller than that of the ultrasonic focus, the resolution of PA imaging is determined by the optical—but not the acoustic—focal size. In this scenario, the technique is often referred to as optical-resolution photoacoustic imaging or microscopy [28,29].

As a hybrid modality, PA imaging takes advantage of the optical contrast and acoustic or optical spatial resolution at moderate tissue depth. Therefore, it has recently seen many fundamental and preclinical trials for the imaging or diagnosis of blood vessels [30], brain [31], breast tumor [32], sentinel lymph node (SLN) [33], oxygen saturation [34], sub-cellular structures [14], and small-animal whole body [35], among many other explorations. While promising, it must be noted that in PA imaging, only the detection of generated ultrasonic signals is "transparent" to tissue; the exciting photons experience the same strong scattering as in other optical microscopic techniques, and the optical fluence decays rapidly with tissue depth. This leads to limited practical depths of PA imaging: for optical resolution schemes, it is curbed to one transport mean free path (~1 mm) [36], beyond which diffusive light dominates and the imaging resolution is no longer determined by the light spot, but the ultrasonic focus; for acoustic resolution schemes, it is curbed to where the in situ optical fluence within the ultrasonic focus is too weak to generate reliable PA signals, usually being a couple of centimeters [13].

Therefore, it would be ideal if the diffusive light can be noninvasively refocused inside or behind thick scattering media. This actually has long been one of the holy grails in the community of biomedical optics. Traditional wisdom has treated multiple scattering of light a nuisance to be bypassed or eliminated. However, recently, researchers began to notice that the seemingly random scattering events and the resultant speckles are actually deterministic within a certain temporal window [37,38], and it is possible to reverse [39–41] or compensate for [42] the scattering-induced phase scrambling. To do so, researchers have developed several wavefront shaping (sometimes also referred to wavefront engineering) techniques, such as iterative wavefront optimization [23–26,28,42–51], measuring the transmission matrix of the scattering medium [21,22,52–56], and optical time reversal via phase conjugation [39,40,57–65]. Nevertheless, the goals of these implementations are identical, i.e., to make light wavelets traveling along different optical paths interfere coherently at a region of interest (ROI) and form a bright optical spot (focus) out of the much darker background.

To create such an optical focus within or inside scattering media, which is more of biomedical interest, an internal guide star is needed to guide or provide a feedback for the wavefront shaping operations. For that purpose, researchers have proposed injected or embedded probes, such as small optical sensors [66,67], fluorescence particles [68,69], and nonlinear beads [57], ultrasound mediation [40,58,61,70,71], as well as absorption perturbation [22,25,46,48,72–76]. Among them, PA signal has been proved very attractive [22,25,28,47,48,53,55,73,74,76], as it is noninvasive, relatively deeply-penetrating, and it can pinpoint the focal spot accurately (the acoustic and optical foci overlap). Furthermore, with linear [22,25,28,53,73,74] or nonlinear [48] PA signals as the guide star, acoustic- and optical-diffraction limited optical focal spot can be achieved, respectively, benefiting from the nature of PA signal generation. In turn, during the process of such PA-guided wavefront optimization,

the in situ optical fluence is gradually increased, and so is the strength of PA signals. Therefore, the signal-to-noise ratio (SNR) and the sensitivity of PA imaging can be greatly enhanced. Moreover, the formation of PA-guided optical focusing at depths in tissue paves the way to break the penetration depth limitation of current acoustic-resolution and optical-resolution PA imaging implementations. This technique, therefore, has the potential to impact the field.

In this paper, we first briefly describe the propagation of light in tissue-like scattering media and the concept of wavefront shaping techniques. Then we discuss, in detail, how PA signals can be used as the guide star for wavefront shaping and how using wavefront shaping can enhance PA imaging in terms of sensitivity and resolution. Lastly, we discuss the existing limitations, challenges, as well as potential solutions in order to advance towards in vivo enhanced PA imaging at depth in tissue.

2. Exploiting Scattering of Light

2.1. Light Scattering in Complex Media and the Memory Effect

In complex media, such as biological tissue samples, spatial inhomogeneities of the wavelength-scale refractive index cause light to be scattered once for every ~100 μm along its optical path. In general, such multiple-scattering feature, according to [19,20], can be described with specific parameters, such as 'mean free path' (MFP) and 'transport mean free path' (TMFP): the former represents the average distance between two consecutive scattering events, and the latter the effective MFP for forward-propagating light portion. Mathematically:

$$l_{MPF} = 1/\mu_s \tag{1}$$

$$l_{TMFP} = 1/[\mu_s(1 - \cos < \theta >)] \tag{2}$$

where μ_s is the scattering coefficient of the medium, and θ is the deflection of angle of the scattered light. Typically, the TMFP of most biological tissues varies from 0.1 to 1 mm. Note that the TMFP of biological tissues is wavelength dependent. Some near-infrared (NIR) light can reach a depth of up to several millimeters [15]; visible light that is widely used in many biomedical techniques only has a shallow penetration depth of hundreds of micrometers inside biological tissue, while a good resolution is sought. Therefore, traditionally scattering events have been regarded as an obstacle, and the speckle patterns generated by the coherent light propagation in tissue has been seen as one of the major noise sources in biomedical optical imaging [77,78]. However, recently, pioneering scientists have begun to explore the feasibility of exploiting scattering and the corresponding speckle patterns based on their deterministic feature within the medium's temporal correlation window [40,63–65].

2.2. Wavefront Shaping

Wavefront shaping is one such technique that scientists have developed. The basic principle is to spatially modulate light incident onto the turbid medium in a way so that scattering-induced phase distortions between the point of incidence and the ROI can be pre-compensated. This technique was first introduced by Vellekoop et al. in 2007 [42]. They used a liquid-crystal-on-silicon (LCoS)-type spatial light modulator (SLM) as the phase/wavefront modulator, with up to 3228 independently controlled pixels to control the phase of every input mode individually. A charge coupled device (CCD) camera was placed to monitor the light intensity at a target position behind a scattering medium. Light intensity reading from the specific CCD pixels was used as the feedback for an optimization algorithm to program the phase patterns on the SLM. In order to maximize the intensity of a chosen area (output mode) recorded by the camera pixels, the phase of each input mode (SLM pixel) was gradually tuned from 0 to 2π. The one that yielded highest feedback was assigned as the optimum phase for that specific SLM pixel. Such iterative optimization process was performed for each SLM pixel. After the optimization, a strong optical focus behind an opaque ground glass diffuser is obtained

(Figure 1b). In comparison, if wavefront shaping is not employed, a fully-randomized speckle pattern is seen (Figure 1a), which is an indicator of sufficient optical diffusion from the medium.

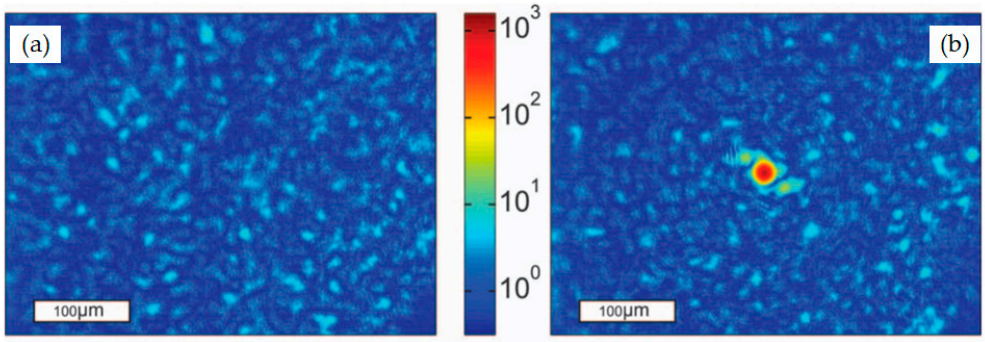

Figure 1. (**a**) A typical optical speckle pattern behind a ground glass diffuser without a shaped incident wavefront; (**b**) Optical pattern of the region with an optimized incident wavefront compensation by using wavefront shaping. A lot of energy of the multiply-scattered light is focused to a spot that is 1000 times brighter than other speckle grains. The size of the optical focus is determined by the sensitivity area of the feedback signal (Figure reproduced from [42]).

Since the initial implementation, wavefront shaping has seen many exciting advancements and has been explored for wide applications, which has been well reviewed [19,79–81] and, thus, will not be reiterated herein. However, it must be pointed out that most efforts in the community have centered on three aspects: to improve the focal intensity enhancement ratio (R), to shorten the optimization process, and to seek appropriate noninvasive guide star to produce the feedback signal. Although the focal enhancement ratio R at the ROI before and after the optimization may vary from case to case (e.g., the working principle of the wavefront modulator), it is overall proportional to $\alpha \times (N/M)$, where N is the number of independently controlled elements on the SLM, M is the number of output modes (speckle grains) within the ROI, and α is a constant depending on the type of wavefront modulator (Table 1). As one can imagine, in order to achieve a high R, a large N and/or small M are required: the former is determined by the technical specification of the wavefront modulator, and the latter by the sensitivity zone of the feedback signal with respect to the speckle grain size. That said, a large N usually requires a longer optimization process [43], which is also significantly affected by the refreshing rate of the wavefront modulator, as well as the speed of data transfer and processing between the sensor, the wavefront modulator, and the processor (usually a personal computer [56]).

Table 1 lists three types of commercial wavefront modulators, i.e., LCoS-type spatial light modulator (SLM), deformable mirror (DM), and digital micromirror device (DMD), that have been popularly used in wavefront shaping. Each has its own advantages and disadvantages; none is perfect. For example, DMD can respond rapidly, but its modulation relies on the tilting of the micro-mirror arrays, and only binary (i.e., either ON or OFF) intensity modulation is supported by DMD. For the other two types, finer steps of phase modulation are usually supported. On the other hand, LCoS-SLM is slow, and DM is expensive and supports small pixel numbers. Therefore, the choosing of a wavefront modulator is usually a trade-off between the speed, the modulation efficiency, the pixel number, and the cost, among many other requirements from the specific application.

Table 1. Representative commercial wavefront modulators [1] (modified from [79]).

Character	LCoS-SLM	DM	DMD
Working principle	Electrically controlled liquid crystal arrays	Piezoelectric arrays and flexible reflective surface	Tilting of micro-mirror arrays
Max pixel number	High (1920 × 1080)	Low (10–1000)	High (3000 × 2000)
Refreshing rate	Slow (10–100 Hz)	Fast (1–10 kHz)	Fast (up to 23 kHz)
Diffraction efficiency	High (60–90%)	High (~100%)	Low (<50%)
Enhancement factor α	$\pi/4$	$\pi/4$	$1/(2\pi)$
Major manufacturer	Holoeye Photonics (German)	Boston Micromachines (USA)	Texas Instruments (USA)
Cost (in US dollar)	Moderate (~20 k)	Moderate (~20 k)	High (~50–100 k)

[1] LCoS, iquid-crystal-on-silicon; SLM, spatial light modulator; DM, deformable mirror; DMD, digital micromirror device.

3. Photoacoustically-Guided Wavefront Shaping (PAWS)

In wavefront shaping, to focus light within a scattering medium, a guide star must be created to produce a feedback signal that is proportional to the in situ optical flux. This could be an actual detector or source, such as a photodiode [27], CCD camera pixel [42], emitting fluorescence molecules [68], or optical nonlinear beads [57]. For biomedical applications, however, using these probes is usually undesired as physical access to the targeted position is required and the embedding procedure of the probes is invasive. Moreover, optical focusing enabled by these physical probes is restricted to fixed positions and cannot be freely moved within tissue. To overcome these limitations, researchers have developed virtual guide stars so that diffused photons emerging or propagating through the ROI can be specifically tagged or preferentially detected. An example is focused ultrasound modulation based on the acousto-optic effect [40,71], where the ultrasonically frequency-shifted photons are phase conjugated and make their way back to the ultrasonic focus—it is, thus, also the optical focus. Similar ultrasonically determined optical focusing can also be achieved if the ultrasonically frequency-shifted photons are extracted and its strength is used as the feedback signal for iterative optimization [27,82,83].

These have inspired the use of photoacoustic signals as the virtual guide star. As discussed earlier, in photoacoustic effect, transient photon energy—no matter it is ballistic or diffusive—is absorbed by tissue molecules and converted into much less scattering ultrasonic waves, which can be detected using a single or a series of transducers. The detected signal can be generally expressed by [48]:

$$\mathrm{PA} = k \iint A(x,y)\Gamma(\mathrm{T})\mu_a F(x,y)dxdy \tag{3}$$

where k is a constant, $A(x,y)$ is the ultrasound detection sensitivity distribution normalized as $\iint A(x,y)dxdy = 1$, Γ is the Grueneisen parameter (usually temperature- and material-dependent), μ_a is the optical absorption coefficient of the local medium, and $F(x,y)$ is the optical energy density (or fluence) within the ultrasonic focus. As seen, when the temperature and the absorption of the ROI remain relatively unchanged, the PA signal amplitude is linearly proportional to the optical fluence F. Therefore, if PA signals are used as the feedback for wavefront shaping, maximizing PA signals' amplitude will lead to maximized optical fluence within the ultrasonic focus and, accordingly, an optical focus inside a highly-scattering medium.

The idea of photoacoustically-guided wavefront shaping (PAWS) was first proposed by Kong et al. in 2011 [25]. As illustrated in Figure 2, they used a 140-pixel deformable mirror (DM) to control the phase of green 1-ns pulses, which were converged by a lens and incident onto a scattering layer. Behind that layer, there were some graphite particles that absorbed diffused pulsed optical energy and generated PA signals, which were detected by a 75 MHz focused ultrasound transducer, amplified, and used as the feedback for optimizing the phase patterns on the DM. Different sizes of graphite absorbers were used to test the capability of optical focusing behind the scattering layer. As a result, a 41 μm-diameter focus was created at the target plane, with an enhancement ratio of 5–10 for the PA signals as well as the focal optical intensity before and after wavefront optimization.

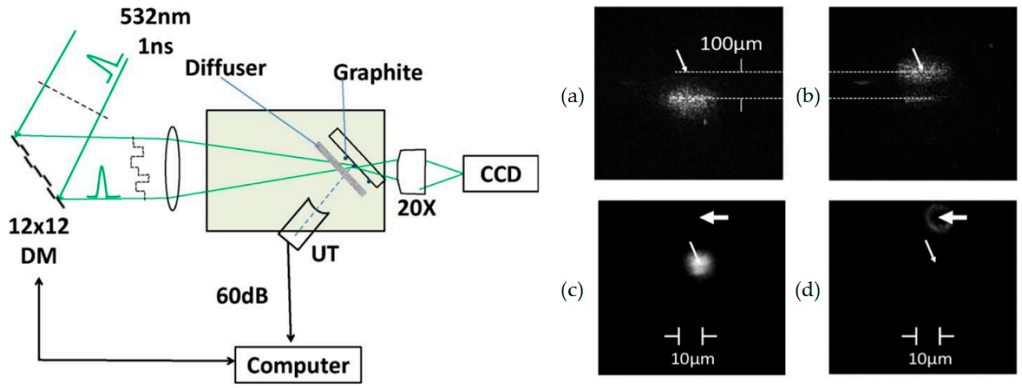

Figure 2. Left: experimental schematic of the first photoacoustically guided optical focusing system. DM, deformable mirror; UT, ultrasound transducer. Right: optical spot behind the scattering layer (**a**) before and (**b**) after being guided to the ultrasonic focal spot (marked by the arrows) via wavefront shaping; (**c**) a photo of graphite particle (marked by wide arrow) after being shifted to 10 μm from the optical beam; and (**d**) the refocused optical beam centered at the graphite particle after wavefront shaping. The narrow arrows mark the locations of the center of ultrasonic focus. The diameter of the ultrasound focus is 90 μm (Figure from ref. [25]).

Using PA signals as the virtual internal guide star has many advantages for biomedical applications. They are noninvasive, label-free, and nontoxic. By translating the ultrasound transducer outside the tissue sample, dynamic optical focusing can be achieved within a large field of view. Moreover, ultrasound has orders of magnitude weaker scattering than light does, and it allows deep penetration and precise pinpointing to the targeted position. Therefore, photoacoustically-guided wavefront shaping has rapidly gained attention and been followed by several other research teams [26,28,45–47]. However, since the diffused optical energy is maximized within the ultrasonic focus, the dimension of the resultant optical focal spot is typically ultrasonic-diffraction limited. For example, the full width of half maximum (FWHM) of the focal zone is ~50 μm for a 50 MHz focused transducer. Within this region, many optical modes exist, resulting in a large M (on the order of 104 considering fully developed speckles) and a limited peak intensity enhancement ratio (inversely proportional to M).

Another promising feature of using photoacoustic signals as the virtual guide star is the capability to break the acoustic diffraction limitation and generate finer resolutions, if nonlinearity in PA signal generation and detection is exploited. For example, it has been demonstrated that sub-acoustic diffraction-limited optical focusing is possible when the detected PA signals (which are broadband) are spectrally filtered and then used as the feedback [26,45]. From the perspective of generation nonlinearity, Lai et al. developed a dual-pulse excitation approach (Figure 3a), firing two consecutive, yet identical, optical pulses to generate two individual PA signals—the difference between them create a nonlinear PA response that can be used as a nonlinear feedback [48]. The hypothesis was built upon a so-called Grueneisen effect [49]. Recall that the PA signal is proportional to the Grueneisen parameter Γ (Equation (3)). For many materials, including water and blood, the value of this parameter increases with in situ temperature within the ultrasonic focus. In this dual-pulse excitation approach, the first laser pulse heated the sample, generating a first PA signal, denoted as PA1; before the first pulse dissipated completely, the second laser pulse was fired, generating a second PA signals denoted as PA2, whose amplitude was larger than PA1 as the value of the corresponding Γ was higher due to the lingering heat. The difference between PA2 and PA1, denoted as ΔPA, is proportional to F2, the square of the optical fluence, instead of F, within the ultrasonic focus. As seen, higher concentration of optical energy onto fewer speckle grains leads to a higher F2 and, hence, a stronger nonlinear PA signal amplitude ΔPA. Therefore, optimization based on such a nonlinear feedback signal strongly

favors energy focusing towards fewer and fewer—eventually a single—optical speckle grain rather than distribution relatively evenly over all speckle grains within the ultrasonic focus.

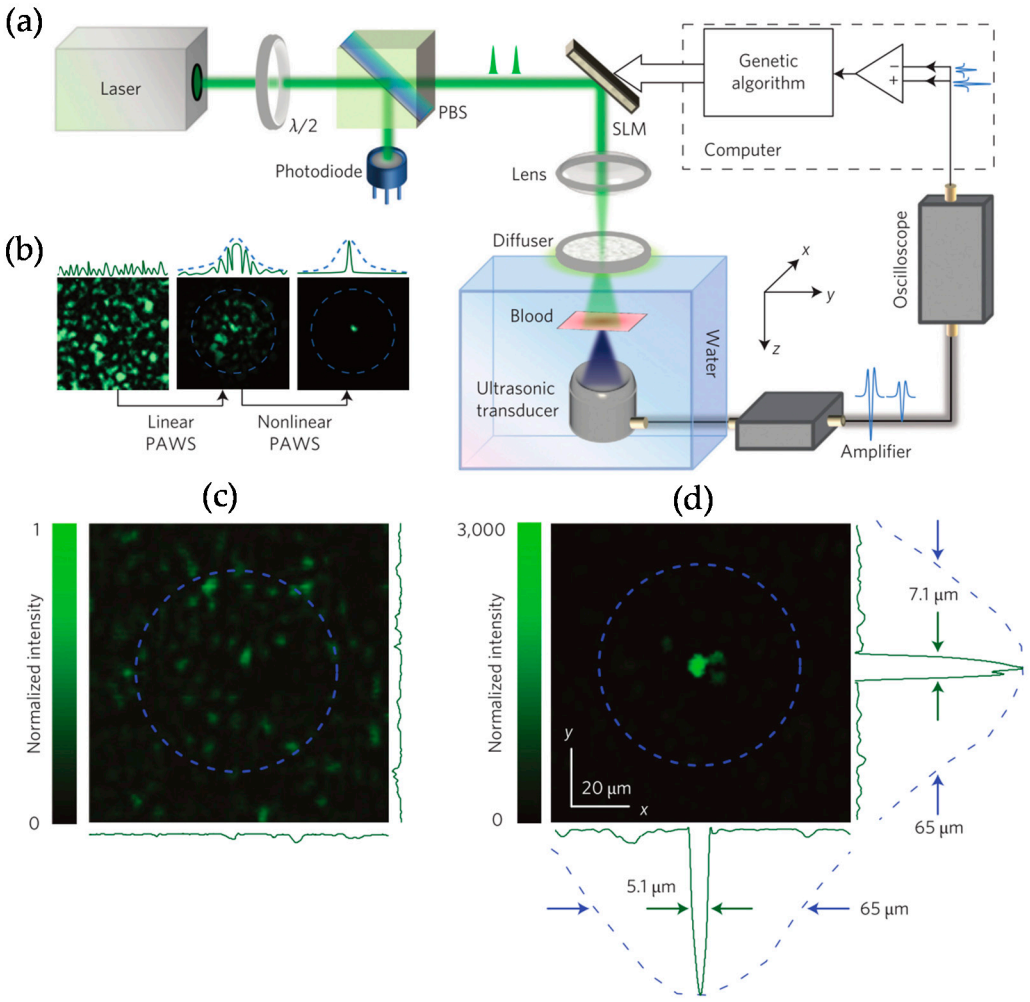

Figure 3. (**a**) Schematic of the two-stage PAWS experimental set-up. λ/2: half-wave plate; PBS: polarizing beam splitter; SLM: LCoS-type spatial light modulator; PAWS, photoacoustically-guided wavefront shaping. (**b**) a representative demonstration for optimization procedure with two stages: linear PAWS focuses light into the acoustic resolution (within the acoustic focal region denoted by blue dashed line); nonlinear PAWS focuses light down to optical resolution (observed as a single-speckle grain); (**c**) the observation upon speckle pattern behind the diffuser without phase modulation (a randomized phase pattern uploaded on the SLM); and (**d**) the optical focus down to optical resolution observed behind the diffuser with phase modulation by nonlinear PAWS (Figure from [48]).

Experimentally, as shown in Figure 3b, regular single-pulse PA signals were first used as the feedback to increase the optical fluence within the ultrasonic focal region, increasing the optical fluence from the initial 0.1 to 6 mJ/cm^2. After that, two optical pulses separated by 40 μs (well within the thermal confinement time of 189 μs under the experimental conditions) were fired every 20 ms. The difference between the two PA signals (ΔPA) was used as the feedback for optimization. Eventually, after iterative optimization a single-speckle grain optical focus, dimensioned at 5–7 μm, was formed around the center of the ultrasonic focal region (Figure 3d), which is about 10 times smaller than the size of the ultrasonic focus. In comparison, before wavefront optimization, or when a random phase pattern was displayed on the SLM, a random speckle pattern was seen, with many speckle grains (~169 through computation) within the ultrasonic focus (Figure 3c). Moreover, the peak optical fluence

improvement ratio from both the linear and nonlinear optimization stages was 60 × 100 = 6000 times, and the peak fluence reached ~600 mJ/cm^2 at the end, which is a really exciting achievement. Such an intensive and tightly focused optical focus within scattering media may benefit many biomedical applications that desire high resolution at depths. For example, a 6000-times improvement in the SNR would make an imaging system much more sensitive and potentially able to image much deeper. Or, if you are doing laser surgery, you could damage targeted tissue much more efficiently, even in deep regions. Surely, this could potentially enable super-resolution photoacoustic imaging in deep tissue.

It needs to be pointed out that the PAWS implementations discussed above all rely on iterative optimization of the feedback signal. In addition to that, there is another version of PAWS to reach the optimum wavefront compensation, i.e., through measuring the optical transmission matrix (TM) of the complex medium. The TM implementation of wavefront shaping was first introduced by Popoff et al. [21], where a CCD camera was used to measure the speckle patterns behind a scattering sample as the output matrix corresponding to specific input modes (SLM modes) (Figure 4). Since the camera can only detect optical intensity, they employed an interferometric approach to simultaneously retrieve both phase and amplitude information of each output mode, with some unmodulated portions as the reference while modulated input modes varying from 0 to 2π independently on the SLM. If all possible input modes on the SLM are visited, the transmission matrix bridging the input and output matrixes can be extracted. With the TM being acquired, arbitrary optical focusing or delivery to any location(s) within the camera's sensing area can be obtained simply by inversing the transmission matrix.

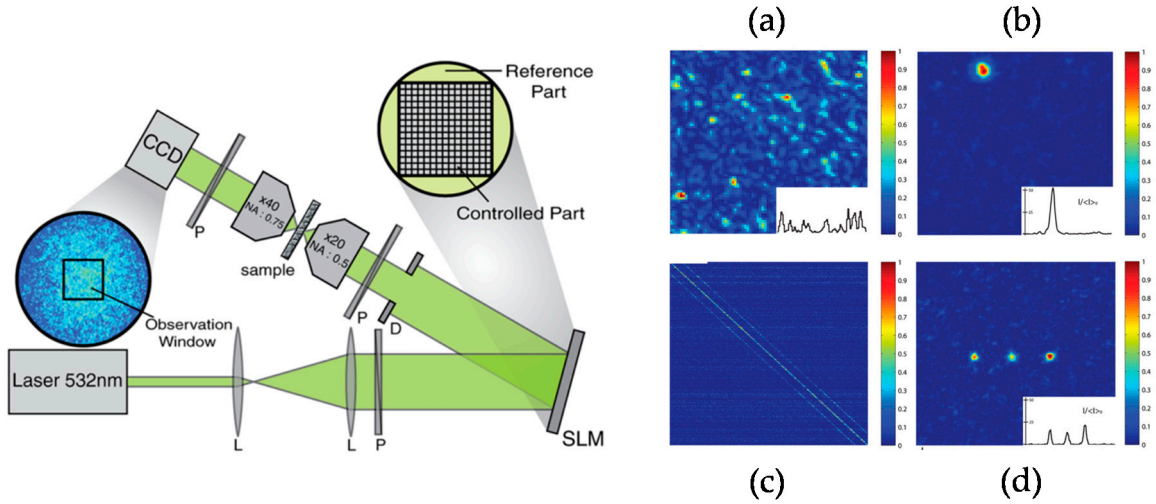

Figure 4. Left: schematic of the experiment. Right: (**a**) the initial optical speckle pattern; (**b**) focusing light onto one focus by measuring the TM with 256 controlled units on the SLM; (**c**) the norm of the focusing operator: each line represents the desired output focusing signal on CCD camera; and (**d**) an example of focusing light onto multiple foci (Figure reproduced from ref. [21]).

Similar to the use of PA signal as feedback in iterative wavefront shaping method, a method called photoacoustic transmission matrix wavefront shaping was developed, using linear PA signal amplitudes as the measured output corresponding to each individual input mode (Figure 5a) [22]. Since photoacoustic signals do not interfere with each other like photons, in order to extract the phase and amplitude information, the authors introduced a new method to get equivalent phase of the output modes to obtain the transmission matrix: the phase of all input modes was set to be identical and scanned from 0 to 2π in 16 steps; each individual photoacoustic signal amplitude from a ultrasound transducer varied and followed a cosine function-like pattern (Figure 5b), from which the photoacoustic transmission matrix can be retrieved. As a result, multiple optical foci can be formed simultaneously by displaying the inversion of the transmission matrix on the SLM screen.

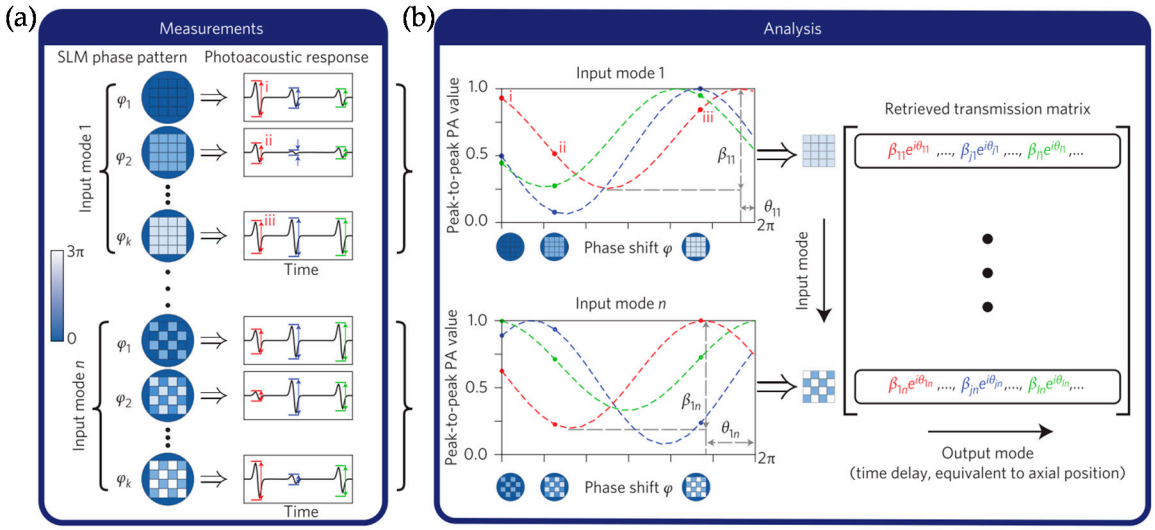

Figure 5. (**a**) The phase of each SLM input mode (in Hadamard basis [84]) is scanned from 0 to 2π in 16 steps; the corresponding photoacoustic trace is measured for each phase step; (**b**) the peak-to-peak amplitude of each PA signal window closely follows a cosine modulation as a function of the phase of an input mode; the photoacoustic transmission-matrix elements are retrieved directly from these cosine modulation phases θij and amplitudes β_{ij} for all input–output mode pairs j, i. The matrix is converted to the SLM-pixel input basis by a basis transformation (Figure from [22]).

4. Enhanced Photoacoustic Imaging with PAWS

Using photoacoustic signal as an internal guide star for wavefront shaping, acoustic-, or optical-diffraction-limited optical focusing can be formed within scattering media. After PAWS, the in situ optical fluence can be greatly increased, and so can be the strength of PA signals. Therefore, PAWS has the potential to enhance the SNR, sensitivity, as well as the imaging resolution and penetration depth of current photoacoustic imaging implementations.

The first demonstration came from Caravaca-Aguirre et al. [28] and Conkey et al. [26], where optical wavefront shaping was combined with genetic algorithm to improve the imaging quality of photoacoustic sensing. The authors [28] placed an absorbing object (two polypropylene 90 µm-inner-diameter tubes filled with India ink) ~8 mm behind a glass diffuser as guidestar for feedback—the distance was calibrated to match the size of photoacoustic focal region with that of a speckle grain. Linear PAWS was firstly used for optimizing the input wavefront to enhance the photoacoustic signal by localizing the optical fluence enhancement. It turned out that a peak-to-peak amplitude enhancement of 10 upon the optimized photoacoustic signal was observed in their study. They, thereby, scanned the absorber with an auto-translation stage in two dimensions around the optimized focus, forming the shown two-dimensional imaging. As for the third dimension, the temporal profile of the ultrasound signal was used to provide the information on that dimension and, hence, the reconstruction of the three-dimensional photoacoustic imaging of the object accordingly. As shown in Figure 6, the PA signal was enhanced by one order of magnitude with PAWS, and the three-dimensional photoacoustic imaging with PAWS shows a much higher SNR and much better well-defined tube structure than that without PAWS.

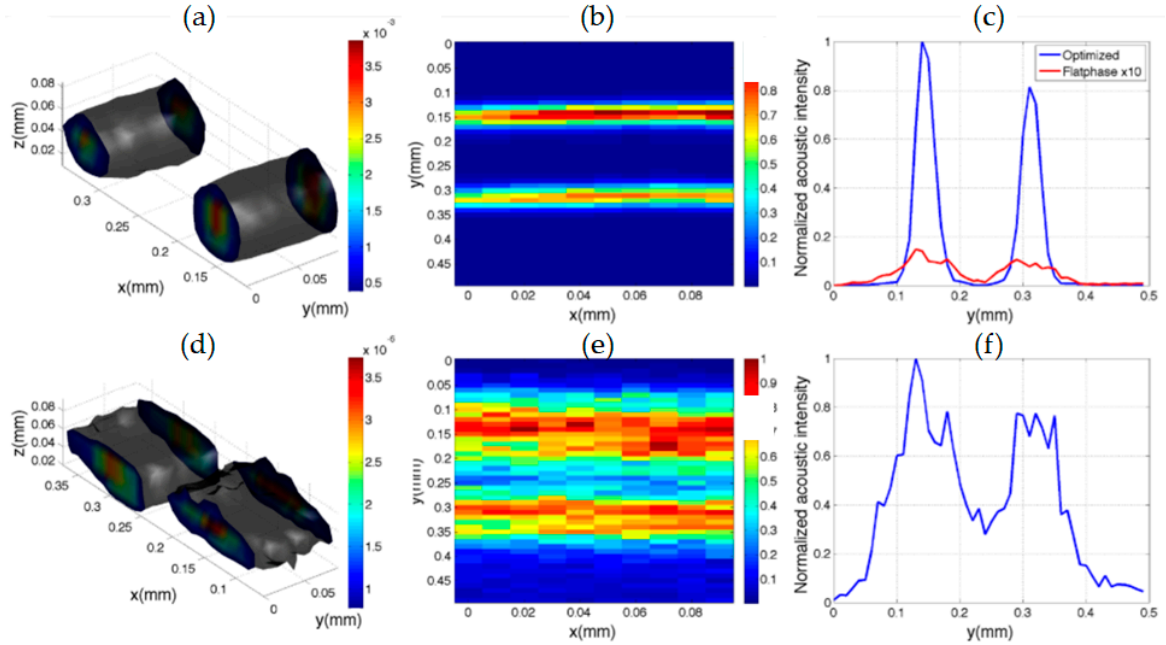

Figure 6. Three-dimensional photoacoustic imaging of two capillary samples: (**a**–**c**) represent the imaging optimized by PAWS; (**d**–**f**) represent the imaging without PAWS by displaying a flat phase pattern on SLM; (**a**,**d**) three-dimensional scan with a 2% intensity threshold regarding the maximum intensity; (**b**,**e**) two-dimensional scan; and (**c**,**f**) 1D scan of the capillary tubes at x = 0.02 mm (Figure from [28]).

The same group also furthered the research to obtain super-resolution photoacoustic imaging [26]. Due to the spatially non-uniformity of acoustic detection (a Gaussian spatial distribution caused by the acoustic focus), optical speckles with higher contribution weighting to the photoacoustic response center more with respect to the center of the acoustic focus. Therefore, photoacoustic signal contributions produced by a single optical speckle near the acoustic focus center are preferentially detected and optimized. As a result, the local intensity of the optical speckle was significantly enhanced (optical enhancement of 24—three times that of the photoacoustic signal amplitude enhancement ratio), whose size is smaller than the acoustic focal size. In the reported experiment, the optical speckle size in the acoustic focus region is 13 µm while the acoustic focus size is 50 µm, which makes it possible to imaging beyond the acoustic resolution. By scanning the sample (without moving the optimized optical focus), an image of a black alpaca hair (25 µm diameter) placed behind a scattering medium with a FWHM of 30 µm was demonstrated in Figure 7a,b. Using the same procedures, they imaged a sweat bee wing, obtaining fine structures and details of the sample (Figure 7g), which is fairly consistent with the scattering-free optical image (Figure 7h) captured by a camera. Furthermore, the authors built a point-by-point image, by scanning the transducer to improve the imaging resolution: an optical focus was optimized and moved from one absorber to another to obtain the spatial responses of photoacoustics. The results (Figure 7c,d) indicate that this method can clearly distinguish individual chromium bars (55 $\pm$ 3 µm wide) after the optimization of PAWS. In the latter case that transducer is used to scan, the ultrasound transducer had a frequency of 50 MHz and an acoustic focal diameter of 61 µm, which apparently wider than the resolution of the PAWS-enabled photoacoustic imaging. Super-resolution in PAWS can also be obtained by using spectral filter detection [45], where a broadband transducer was used for sensing photoacoustic signals, which were high-pass filtered and used as feedback PAWS optimization. This study unveils non-uniform PAWS focusing capability regardless of different photoacoustic spectra and focusing enhancement ratio. Although not directly shown, this method could be helpful in enhancing the sensitivity, as well as the resolution of photoacousic imaging.

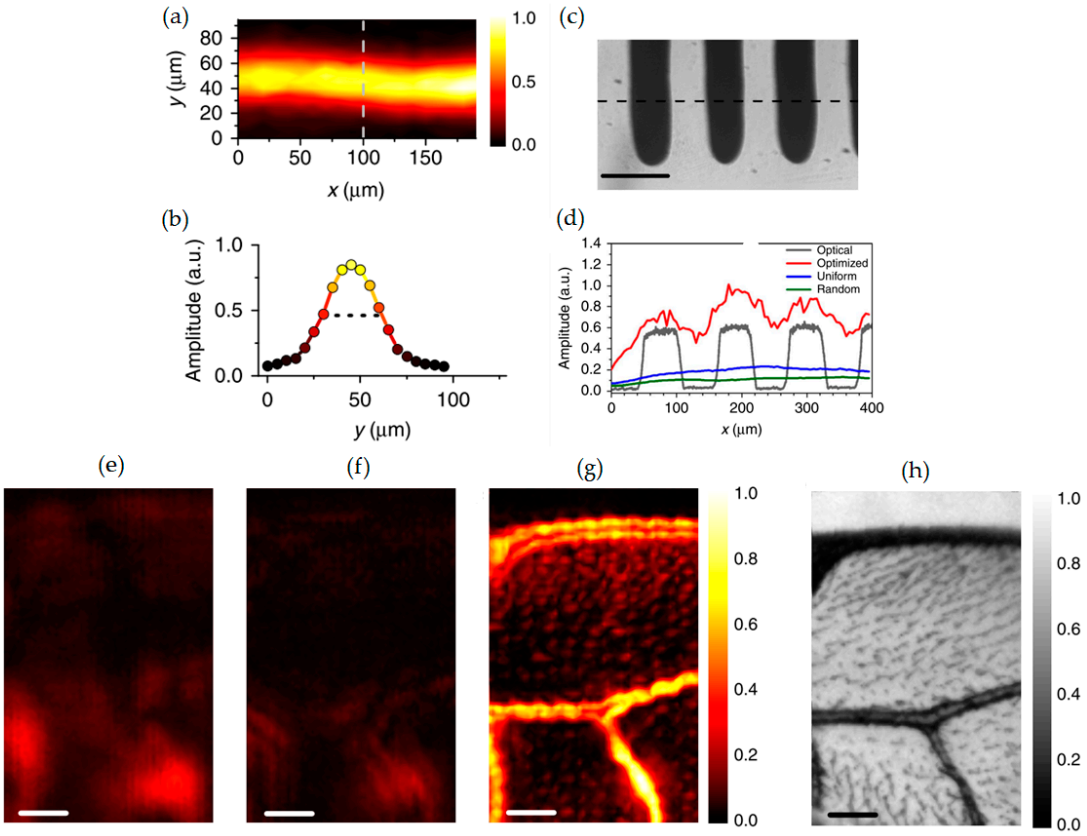

Figure 7. Super-resolution photoacoustic imaging. Scale bar: 100 μm. (**a**) Photoacoustic image of a black alpaca hair (25 μm diameter) and (**b**) PA signal intensity profile along the dashed line in (**a**), showing a diameter of 30 μm defined by the full width of half maximum (FWHM). (**c**) Direct microscopic image of multiple hairs. (**d**) Experimental one-dimensional (1D) scan images with direct optical microscopic, and with uniform, random, and optimized phase compensations, repsctively. (**e**–**g**) Sweat bee wing images with uniform, random speckle, as well as optimized wavefront illuminations, respectively. (**h**) Direction microscopic image of the bee wing serves as the gold standard for comparison. (Figure from [26]).

The aforementioned enhanced PA imaging cases were all implemented based on iterative PAWS optimization. Chaigne et al. [53] recently showed that similar PA imaging enhancement could be obtained by measuring the photoacoustic transmission matrix of the complex medium, following a protocol from [22] by applying cosine modulations to the photoacoustic signals. In their approach (Figure 8), a black leaf skeleton was placed behind a ground glass diffuser as an optical absorber, in order to generate photoacoustic signals used as feedback. The PA signals were detected by a linear ultrasound array (15 MHz central frequency). The hypothesis is that all optical information had been well included in the transmission matrix, so that the photoacoustic image could be reconstructed without any additional measurements. By analyzing the modulation, the authors successfully reconstructed detailed infrastructure of the leaf skeleton (Figure 8e), which is consistent and comparable with the skeleton information provided by a photograph of the same leaf captured by a CCD camera in a scattering-free setting (Figure 8b). Compared with the standard photoacoustic images by various speckle illuminations (Figure 8b,c), the enhancement in imaging quality is quite obvious.

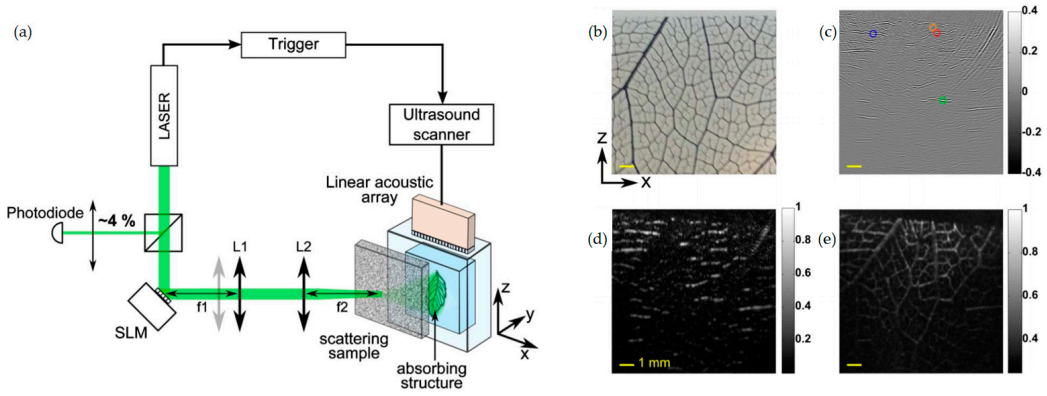

Figure 8. (**a**) Experimental setup for PAWS (transmission matrix measurement approach); (**b**) reference photograph of the absorbing leaf skeleton embedded in a transparent agarose gel block; (**c**) a standard photoacoustic image obtained by averaging different speckle illuminations and its envelope (**d**); and (**e**) enhanced photoacoustic imaging with PAWS optimization.

5. Discussion and Conclusions

It has been shown that that using photoacoustic signals as feedback for optical wavefront shaping techniques open up a new road to focus scattering light within or behind tissue samples or optically-scattering media, which can in turn be used to increase the sensitivity, the resolution and, potentially, the penetration depth of photoacoustic imaging. The dissipation limit of PAT is several cm. By converging diffused energy into region of interest in deep tissue, wavefront shaping is able to break this limit, and eventually made suitable for whole-body imaging. For optical-resolution PAM (OR-PAM), wavefront shaping may be more attractive in that the diffusion limit can be surpassed, and the penetration depth can be up to several millimeters. Such integration may result in the critical impact to the diagnosis and treatment of diseases that exhibit direct or indirect optical contrast. To make it more practical towards biomedical applications in vivo, however, several challenges must be tackled.

The first one is the speed of optical focusing. For example, the above-discussed nonlinear PAWS implementation [48] took several hours to complete a phase compensation optimization and produce the shown intense single speckle-scale optical focus. This time-consuming drawback is mainly due to the inherent requirement of many signal measurements and phase pattern update. Using an LCoS-type SLM whose refresh rate is 60 Hz, each iteration takes about one second, as reported [42,48], which is mainly throttled by the refresh rate of the SLM, the inability of the Windows® operation system for parallel signal processing, as well as the communication speed between the PC and the SLM. Therefore, a fast substitute is in demand for practical applications, especially with living biological tissue, whose decorrelation time is typically a few milliseconds, or even shorter [40]. One straight-forward solution is to use DMD (refresh rate can be up to 23 kHz) in place of the LCoS-type SLM, and a field programmable gate array (FPGA) in place of the PC processor to significantly shorten the time needed to update the phase patterns, as well as data communication and processing for each iteration. Promising improvement of the iterative optimization speed has been confirmed [24,56]. It should be noted, however, that the modulation from DMD relies on the tilting of the micro-mirror arrays, and only binary (i.e., either ON or OFF) intensity modulation is supported. Thus, usually a sacrificed enhancement ratio can be delivered compared to when an LCoS-type SLM serves as the wavefront modulator. Nevertheless, there is no doubt that a higher optimization speed, such as accomplishing thousands of iterations within one second, is critical to allow for practical applications of interest.

With the abovementioned methods, generating one single optical focus with increased optimization speed is feasible. Yet, in many applications, including photoacoustic microscopy, a series of optical focal points are needed and rapid raster scanning of optical foci is required. Can the

PAWS-generated focal spot be translated sufficiently fast? Note that tissue constituents and the corresponding optimized phase compensation vary spatially, and a new cycle of iterations may be needed from one position to another. Using the so-called memory effect (a speckle correlation phenomenon) [37,38], it is possible to tilt the obtained phase pattern by a small angle, which can translate the focus across the focal plane and is, thus, useful in eliminating the need for a new full optimization process at each point. However, the effective rotation range is only a few milliradians in the targeted scenario. Beyond that, the new position is far away from the initial focus, the phase compensation difference is no longer "geometrical" as expressed by the memory effect, and the phase pattern on the DMD must be updated accordingly. One potential solution is to measure the transmission matrix of the experimental sample in advance [53]. Through manipulating the transmission matrix, we are able to "raster" scan the optical focus and, hence, form 2D or 3D PA images, within a field of view that is much larger than the optical focal spot size [21,22,53]. Measurement of the transmission matrix and the scanning speed are only limited by the refreshing rate of the DMD; there is no need to perform a full process of iterations or transmission matrix measurements for each individual point. This can greatly reduce the data transfer and computation burden on the processor, until the studied sample has moved or changed that significantly alters the transmission matrix.

Faster optimization may also allow for higher focal enhancement ratio R at the ROI before and after the optimization, which is imperative for many applications that desire intensive and tightly-focused light delivery within tissue. As discussed earlier, the enhancement ratio is proportional to N/M [80], i.e., the more is the input modes N on the wavefront modulator, the higher R can be. For example, Lai et al. [48] used N = 192 × 108 on an SLM and obtained a focal enhancement ratio of ~6000, with an optimization process of several hours. Slow speed has prevented this implementation from further applications. More recently, Yu et al. [56] used megapixels on a DMD and achieved an enhancement ratio of >100,000, with an optimization process slightly longer than one hour, even though a much higher N was employed. This will not be possible without the use of a much faster-responding modulator DMD, even though the full power of the DMD has not been released yet and the focusing speed can be further improved.

In conclusion, using photoacoustic signal as a virtual internal guide star allows for acoustic- or optical-diffraction limited optical focusing with an intensive focal-to-background ratio within biological tissue or tissue-like media. With further engineered, PAWS can be a promising tool to bring the sensitivity, the resolution, and potentially the penetration depth of existing photoacoustic imaging implementations to a new level.

Acknowledgments: The work has been supported by the Hong Kong Research Grant Council (no. 252044/16E) and the National Natural Science Foundation of China (no. 81671726 and no. 81627805)

Author Contributions: Zhipeng Yu initiated the manuscript. All authors participated in the revision of the manuscript. Puxiang Lai provided overall supervision.

Conflicts of Interest: The authors declare no conflict of interest.

References

1. Huang, D.; Swanson, E.A.; Lin, C.P.; Schuman, J.S.; Stinson, W.G.; Chang, W.; Hee, M.R.; Flotte, T.; Gregory, K.; Puliafito, C.A.; et al. Optical coherence tomography. *Science* **1991**, *254*, 1178–1181. [CrossRef] [PubMed]
2. Pawley, J.B. *Handbook of Biological Confocal Microscopy*, 3rd ed.; Springer: Berlin, Germany, 2006.
3. Beaurepaire, E.; Oheim, M.; Mertz, J. Ultra-deep two-photon fluorescence excitation in turbid media. *Opt. Commun.* **2001**, *188*, 25–29. [CrossRef]
4. Theer, P.; Hasan, M.T.; Denk, W. Two-photon imaging to a depth of 1000 µm in living brains by use of a Ti: Al_2O_3 regenerative amplifier. *Opt. Lett.* **2003**, *28*, 1022–1024. [CrossRef] [PubMed]
5. Helmchen, F.; Denk, W. Deep tissue two-photon microscopy. *Nat. Methods* **2005**, *2*, 932–940. [CrossRef] [PubMed]

6. Sakadžić, S.; Demirbas, U.; Mempel, T.R.; Moore, A.; Ruvinskaya, S.; Boas, D.A.; Sennaroglu, A.; Kartner, F.X.; Fujimoto, J.G. Multi-photon microscopy with a low-cost and highly efficient Cr: LiCAF laser. *Opt. Express* **2008**, *16*, 20848–20863. [CrossRef] [PubMed]
7. Kobat, D.; Horton, N.G.; Xu, C. In vivo two-photon microscopy to 1.6 mm depth in mouse cortex. *J. Biomed. Opt.* **2011**, *16*, 106014. [CrossRef] [PubMed]
8. Horton, N.G.; Wang, K.; Kobat, D.; Clark, C.G.; Wise, F.W.; Schaffer, C.B.; Xu, C. In vivo three-photon microscopy of subcortical structures within an intact mouse brain. *Nat. Photonics* **2013**, *7*, 205–209. [CrossRef] [PubMed]
9. Betzig, E.; Patterson, G.H.; Sougrat, R.; Lindwasser, O.W.; Olenych, S.; Bonifacino, J.S.; Davidson, M.W.; Lippincott-Schwartz, J.; Hess, H.F. Imaging intracellular fluorescent proteins at nanometer resolution. *Science* **2006**, *313*, 1642. [CrossRef] [PubMed]
10. Willig, K.I.; Rizzoli, S.O.; Westphal, V.; Jahn, R.; Hell, S.W. STED microscopy reveals that synaptotagmin remains clustered after synaptic vesicle exocytosis. *Nature* **2006**, *440*, 935–939. [CrossRef] [PubMed]
11. Tuchin, V.V.; Tuchin, V. *Tissue Optics: Light Scattering Methods and Instruments for Medical Diagnosis*; SPIE Press: Bellingham, WA, USA, 2007.
12. Ntziachristos, V.; Razansky, D. Molecular imaging by means of multispectral optoacoustic tomography (MSOT). *Chem. Rev.* **2010**, *110*, 2783–2794. [CrossRef] [PubMed]
13. Beard, P. Biomedical photoacoustic imaging. *Interface Focus* **2011**, *1*, 602–631. [CrossRef] [PubMed]
14. Wang, L.V.; Hu, S. Photoacoustic tomography: In vivo imaging from organelles to organs. *Science* **2012**, *335*, 1458–1462. [CrossRef] [PubMed]
15. Wang, L.V.; Wu, H.I. *Biomedical Optics: Principles and Imaging*; John Wiley & Sons: Hoboken, NJ, USA, 2012.
16. Kruger, R.A. Photoacoustic ultrasound. *Med. Phys.* **1994**, *21*, 127–131. [CrossRef] [PubMed]
17. Karabutov, A.; Podymova, N.; Letokhov, V. Time-resolved laser optoacoustic tomography of inhomogeneous media. *Appl. Phys. B* **1996**, *63*, 545–563. [CrossRef]
18. Oraevsky, A.A.; Jacques, S.L.; Tittel, F.K. Measurement of tissue optical properties by time-resolved detection of laser-induced transient stress. *Appl. Opt.* **1997**, *36*, 402–415. [CrossRef] [PubMed]
19. Mosk, A.P.; Lagendijk, A.; Lerosey, G.; Fink, M. Controlling waves in space and time for imaging and focusing in complex media. *Nat. Photonics* **2012**, *6*, 283–292. [CrossRef]
20. Popoff, S.; Lerosey, G.; Fink, M.; Boccara, A.C.; Gigan, S. Image transmission through an opaque material. *Nat. Commun.* **2010**, *1*, 81. [CrossRef] [PubMed]
21. Popoff, S.; Lerosey, G.; Carminati, R.; Fink, M.; Boccara, A.; Gigan, S. Measuring the transmission matrix in optics: An approach to the study and control of light propagation in disordered media. *Phys. Rev. Lett.* **2010**, *104*, 100601. [CrossRef] [PubMed]
22. Chaigne, T.; Katz, O.; Boccara, A.C.; Fink, M.; Bossy, E.; Gigan, S. Controlling light in scattering media non-invasively using the photoacoustic transmission matrix. *Nat. Photonics* **2014**, *8*, 58–64. [CrossRef]
23. Conkey, D.B.; Brown, A.N.; Caravaca-Aguirre, A.M.; Piestun, R. Genetic algorithm optimization for focusing through turbid media in noisy environments. *Opt. Express* **2012**, *20*, 4840–4849. [CrossRef] [PubMed]
24. Conkey, D.B.; Caravaca-Aguirre, A.M.; Piestun, R. High-speed scattering medium characterization with application to focusing light through turbid media. *Opt. Express* **2012**, *20*, 1733–1740. [CrossRef] [PubMed]
25. Kong, F.; Silverman, R.H.; Liu, L.; Chitnis, P.V.; Lee, K.K.; Chen, Y.C. Photoacoustic-guided convergence of light through optically diffusive media. *Opt. Lett.* **2011**, *36*, 2053–2055. [CrossRef] [PubMed]
26. Conkey, D.B.; Caravaca-Aguirre, A.M.; Dove, J.D.; Ju, H.Y.; Murray, T.W.; Piestun, R. Super-resolution photoacoustic imaging through a scattering wall. *Nat. Commun.* **2015**, *6*, 1. [CrossRef] [PubMed]
27. Tay, J.W.; Lai, P.X.; Suzuki, Y.; Wang, L.V. Ultrasonically encoded wavefront shaping for focusing into random media. *Sci. Rep.* **2014**, *4*, 5. [CrossRef] [PubMed]
28. Caravaca-Aguirre, A.M.; Conkey, D.B.; Dove, J.D.; Ju, H.; Murray, T.W.; Piestun, R. High contrast three-dimensional photoacoustic imaging through scattering media by localized optical fluence enhancement. *Opt. Express* **2013**, *21*, 26671–26676. [CrossRef] [PubMed]
29. Yao, J.; Wang, L.V. Photoacoustic Microscopy. *Laser Photonics Rev.* **2013**, *7*. [CrossRef] [PubMed]
30. Hoelen, C.; de Mul, F.; Pongers, R.; Dekker, A. Three-dimensional photoacoustic imaging of blood vessels in tissue. *Opt. Lett.* **1998**, *23*, 648–650. [CrossRef] [PubMed]

31. Wang, X.; Pang, Y.; Ku, G.; Xie, X.; Stoica, G.; Wang, L.V. Noninvasive laser-induced photoacoustic tomography for structural and functional in vivo imaging of the brain. *Nat. Biotechnol.* **2003**, *21*, 803–806. [CrossRef] [PubMed]
32. Xi, L.; Grobmyer, S.R.; Wu, L.; Chen, R.; Zhou, G.; Gutwein, L.G.; Sun, J.; Liao, W.; Zhou, Q.; Xie, H. Evaluation of breast tumor margins in vivo with intraoperative photoacoustic imaging. *Opt. Express* **2012**, *20*, 8726–8731. [CrossRef] [PubMed]
33. Song, K.H.; Kim, C.; Cobley, C.M.; Xia, Y.; Wang, L.V. Near-infrared gold nanocages as a new class of tracers for photoacoustic sentinel lymph node mapping on a rat model. *Nano Lett.* **2009**, *9*, 183–188. [CrossRef] [PubMed]
34. Zhang, H.F.; Maslov, K.; Sivaramakrishnan, M.; Stoica, G.; Wang, L.V. Imaging of hemoglobin oxygen saturation variations in single vessels in vivo using photoacoustic microscopy. *Appl. Phys. Lett.* **2007**, *90*, 053901. [CrossRef]
35. Xia, J.; Wang, L.V. Small-animal whole-body photoacoustic tomography: A review. *IEEE Trans. Biomed. Eng.* **2014**, *61*, 1380–1389. [PubMed]
36. Maslov, K.; Zhang, H.F.; Hu, S.; Wang, L.V. Optical-resolution photoacoustic microscopy for in vivo imaging of single capillaries. *Opt. Lett.* **2008**, *33*, 929–931. [CrossRef] [PubMed]
37. Freund, I.; Rosenbluh, M.; Feng, S. Memory effects in propagation of optical waves through disordered media. *Phys. Rev. Lett.* **1988**, *61*, 2328–2331. [CrossRef] [PubMed]
38. Feng, S.; Kane, C.; Lee, P.A.; Stone, A.D. Correlations and fluctuations of coherent wave transmission through disordered media. *Phys. Rev. Lett.* **1988**, *61*, 834. [CrossRef] [PubMed]
39. Ma, C.; Zhou, F.; Liu, Y.; Wang, L.V. Single-exposure optical focusing inside scattering media using binarized time-reversed adapted perturbation. *Optica* **2015**, *2*, 869–876. [CrossRef]
40. Liu, Y.; Lai, P.; Ma, C.; Xu, X.; Grabar, A.A.; Wang, L.V. Optical focusing deep inside dynamic scattering media with near-infrared time-reversed ultrasonically encoded (TRUE) light. *Nat. Commun.* **2015**, *6*, 5904. [CrossRef] [PubMed]
41. Yaqoob, Z.; Psaltis, D.; Feld, M.S.; Yang, C. Optical phase conjugation for turbidity suppression in biological samples. *Nat. Photonics* **2008**, *2*, 110–115. [CrossRef] [PubMed]
42. Vellekoop, I.M.; Mosk, A. Focusing coherent light through opaque strongly scattering media. *Opt. Lett.* **2007**, *32*, 2309–2311. [CrossRef] [PubMed]
43. Vellekoop, I.M.; Mosk, A.P. Phase control algorithms for focusing light through turbid media. *Opt. Commun.* **2008**, *281*, 3071–3080. [CrossRef]
44. Akbulut, D.; Huisman, T.J.; van Putten, E.G.; Vos, W.L.; Mosk, A.P. Focusing light through random photonic media by binary amplitude modulation. *Opt. Express* **2011**, *19*, 4017–4029. [CrossRef] [PubMed]
45. Chaigne, T.; Gateau, J.; Katz, O.; Boccara, C.; Gigan, S.; Bossy, E. Improving photoacoustic-guided optical focusing in scattering media by spectrally filtered detection. *Opt. Lett.* **2014**, *39*, 6054–6057. [CrossRef] [PubMed]
46. Deán-Ben, X.L.; Estrada, H.; Razansky, D. Shaping volumetric light distribution through turbid media using real-time three-dimensional opto-acoustic feedback. *Opt. Lett.* **2015**, *40*, 443–446. [CrossRef] [PubMed]
47. Tay, J.W.; Liang, J.; Wang, L.V. Amplitude-masked photoacoustic wavefront shaping and application in flowmetry. *Opt. Lett.* **2014**, *39*, 5499–5502. [CrossRef] [PubMed]
48. Lai, P.; Wang, L.; Tay, J.W.; Wang, L.V. Photoacoustically guided wavefront shaping for enhanced optical focusing in scattering media. *Nat. Photonics* **2015**, *9*, 126–132. [CrossRef] [PubMed]
49. Wang, L.; Zhang, C.; Wang, L.V. Grueneisen relaxation photoacoustic microscopy. *Phys. Rev. Lett.* **2014**, *113*, 174301. [CrossRef] [PubMed]
50. Katz, O.; Small, E.; Guan, Y.; Silberberg, Y. Noninvasive nonlinear focusing and imaging through strongly scattering turbid layers. *Optica* **2014**, *1*, 170–174. [CrossRef]
51. Tang, J.; Germain, R.N.; Cui, M. Superpenetration optical microscopy by iterative multiphoton adaptive compensation technique. *Proc. Natl. Acad. Sci. USA* **2012**, *109*, 8434–8439. [CrossRef] [PubMed]
52. Katz, O.; Ramaz, F.; Gigan, S.; Fink, M. Controlling light in complex media beyond the acoustic diffraction-limit using the acousto-optic transmission matrix. *arXiv* **2017**.
53. Chaigne, T.; Gateau, J.; Katz, O.; Bossy, E.; Gigan, S. Light focusing and two-dimensional imaging through scattering media using the photoacoustic transmission matrix with an ultrasound array. *Opt. Lett.* **2014**, *39*, 2664–2667. [CrossRef] [PubMed]

54. Drémeau, A.; Liutkus, A.; Martina, D.; Katz, O.; Schülke, C.; Krzakala, F.; Gigan, S.; Daudet, L. Reference-less measurement of the transmission matrix of a highly scattering material using a DMD and phase retrieval techniques. *Opt. Express* **2015**, *23*, 11898–11911. [CrossRef] [PubMed]
55. Abe, H.; Shiina, T. Visualization of photoacoustic images in a limited-View measuring system using eigenvalues of a photoacoustic transmission matrix. *Photoacoustics* **2017**, *8*, 1–7. [CrossRef] [PubMed]
56. Yu, H.; Lee, K.; Park, Y. Ultrahigh enhancement of light focusing through disordered media controlled by mega-pixel modes. *Opt. Express* **2017**, *25*, 8036–8047. [CrossRef] [PubMed]
57. Hsieh, C.L.; Pu, Y.; Grange, R.; Laporte, G.; Psaltis, D. Imaging through turbid layers by scanning the phase conjugated second harmonic radiation from a nanoparticle. *Opt. Express* **2010**, *18*, 20723–20731. [CrossRef] [PubMed]
58. Judkewitz, B.; Wang, Y.M.; Horstmeyer, R.; Mathy, A.; Yang, C.H. Speckle-scale focusing in the diffusive regime with time reversal of variance-encoded light (TROVE). *Nat. Photonics* **2013**, *7*, 300–305. [CrossRef] [PubMed]
59. Ma, C.; Xu, X.; Liu, Y.; Wang, L.V. Time-reversed adapted-perturbation (TRAP) optical focusing onto dynamic objects inside scattering media. *Nat. Photonics* **2014**, *8*, 931–936. [CrossRef] [PubMed]
60. Zhou, E.H.; Ruan, H.W.; Yang, C.H.; Judkewitz, B. Focusing on moving targets through scattering samples. *Optica* **2014**, *1*, 227–232. [CrossRef] [PubMed]
61. Ruan, H.W.; Jang, M.; Yang, C.H. Optical focusing inside scattering media with time-reversed ultrasound microbubble encoded light. *Nat. Commun.* **2015**, *6*, 8. [CrossRef] [PubMed]
62. Shen, Y.; Liu, Y.; Ma, C.; Wang, L.V. Focusing light through biological tissue and tissue-mimicking phantoms up to 9.6 cm in thickness with digital optical phase conjugation. *J. Biomed. Opt.* **2016**, *21*, 085001. [CrossRef] [PubMed]
63. Wang, D.; Zhou, E.H.; Brake, J.; Ruan, H.; Jang, M.; Yang, C. Focusing through dynamic tissue with millisecond digital optical phase conjugation. *Optica* **2015**, *2*, 728–735. [CrossRef] [PubMed]
64. Jang, M.; Ruan, H.; Vellekoop, I.M.; Judkewitz, B.; Chung, E.; Yang, C. Relation between speckle decorrelation and optical phase conjugation (OPC)-based turbidity suppression through dynamic scattering media: A study on in vivo mouse skin. *Biomed. Opt. Express* **2015**, *6*, 72–85. [CrossRef] [PubMed]
65. Liu, Y.; Ma, C.; Shen, Y.; Shi, J.; Wang, L.V. Focusing light inside dynamic scattering media with millisecond digital optical phase conjugation. *Optica* **2017**, *4*, 280–288. [CrossRef] [PubMed]
66. Thompson, J.V.; Throckmorton, G.A.; Hokr, B.H.; Yakovlev, V.V. Wavefront shaping enhanced Raman scattering in a turbid medium. *Opt. Lett.* **2016**, *41*, 1769–1772. [CrossRef] [PubMed]
67. Suzuki, Y.; Tay, J.W.; Yang, Q.; Wang, L.V. Continuous scanning of a time-reversed ultrasonically encoded optical focus by reflection-mode digital phase conjugation. *Opt. Lett.* **2014**, *39*, 3441–3444. [CrossRef] [PubMed]
68. Vellekoop, I.M.; Cui, M.; Yang, C. Digital optical phase conjugation of fluorescence in turbid tissue. *Appl. Phys. Lett.* **2012**, *101*, 081108. [CrossRef] [PubMed]
69. Wang, Y.M.; Judkewitz, B.; DiMarzio, C.A.; Yang, C. Deep-tissue focal fluorescence imaging with digitally time-reversed ultrasound-encoded light. *Nat. Commun.* **2012**, *3*, 928. [CrossRef] [PubMed]
70. Xu, X.; Liu, H.; Wang, L.V. Time-reversed ultrasonically encoded optical focusing into scattering media. *Nat. Photonics* **2011**, *5*, 154–157. [CrossRef] [PubMed]
71. Lai, P.; Suzuki, Y.; Xu, X.; Wang, L.V. Focused fluorescence excitation with time-reversed ultrasonically encoded light and imaging in thick scattering media. *Laser Phys. Lett.* **2013**, *10*, 075604. [CrossRef] [PubMed]
72. Konstantinou, G.; Kirkby, P.A.; Evans, G.J.; Nadella, K.N.S.; Griffiths, V.A.; Mitchell, J.E.; Silver, R.A. Dynamic wavefront shaping with an acousto-optic lens for laser scanning microscopy. *Opt. Express* **2016**, *24*, 6283–6299. [CrossRef] [PubMed]
73. Dean-Ben, X.L.; Estrada, H.; Ozbek, A.; Razansky, D. Influence of the absorber dimensions on wavefront shaping based on volumetric optoacoustic feedback. *Opt. Lett.* **2015**, *40*, 5395–5398. [CrossRef] [PubMed]
74. Gao, F.; Feng, X.; Zhang, R.; Liu, S.; Ding, R.; Kishor, R.; Zheng, Y. Single laser pulse generates dual photoacoustic signals for differential contrast photoacoustic imaging. *Sci. Rep.* **2017**, *7*, 626. [CrossRef] [PubMed]
75. Tzang, O.; Niv, E.; Caravaca-Aguirre, A.M.; Piestun, R. Thermal expansion feedback for wave-front shaping. *Opt. Express* **2017**, *25*, 6122–6131. [CrossRef] [PubMed]

76. Tzang, O.; Piestun, R. Lock-in detection of photoacoustic feedback signal for focusing through scattering media using wave-front shaping. *Opt. Express* **2016**, *24*, 28122–28130. [CrossRef] [PubMed]
77. Goodman, J.W. *Statistical Optics*; John Wiley & Sons: Hoboken, NJ, USA, 2015.
78. Goodman, J.W. *Speckle Phenomena in Optics: Theory and Applications*; Roberts and Company Publishers: Greenwood Village, CO, USA, 2007.
79. Yu, H.; Park, J.; Lee, K.; Yoon, J.; Kim, K.; Lee, S.; Park, Y. Recent advances in wavefront shaping techniques for biomedical applications. *Curr. Appl. Phys.* **2015**, *15*, 632–641. [CrossRef]
80. Vellekoop, I.M. Feedback-based wavefront shaping. *Opt. Express* **2015**, *23*, 12189–12206. [CrossRef] [PubMed]
81. Horstmeyer, R.; Ruan, H.; Yang, C. Guidestar-assisted wavefront-shaping methods for focusing light into biological tissue. *Nat. Photonics* **2015**, *9*, 563–571. [CrossRef] [PubMed]
82. Ruan, H.; Jang, M.; Judkewitz, B.; Yang, C. Iterative time-reversed ultrasonically encoded light focusing in backscattering mode. *Sci. Rep.* **2014**, *4*, 7156. [CrossRef] [PubMed]
83. Si, K.; Fiolka, R.; Cui, M. Breaking the spatial resolution barrier via iterative sound-light interaction in deep tissue microscopy. *Sci. Rep.* **2012**, *2*, 748. [CrossRef] [PubMed]
84. Yarlagadda, R.K.; Hershey, J.E. *Hadamard Matrix Analysis and Synthesis: With Applications to Communications and Signal/Image Processing*; Springer Science & Business Media: Berlin, Germany, 2012.